

Nanoscale

Accepted Manuscript



This is an *Accepted Manuscript*, which has been through the RSC Publishing peer review process and has been accepted for publication.

Accepted Manuscripts are published online shortly after acceptance, which is prior to technical editing, formatting and proof reading. This free service from RSC Publishing allows authors to make their results available to the community, in citable form, before publication of the edited article. This *Accepted Manuscript* will be replaced by the edited and formatted *Advance Article* as soon as this is available.

To cite this manuscript please use its permanent Digital Object Identifier (DOI®), which is identical for all formats of publication.

More information about *Accepted Manuscripts* can be found in the [Information for Authors](#).

Please note that technical editing may introduce minor changes to the text and/or graphics contained in the manuscript submitted by the author(s) which may alter content, and that the standard [Terms & Conditions](#) and the [ethical guidelines](#) that apply to the journal are still applicable. In no event shall the RSC be held responsible for any errors or omissions in these *Accepted Manuscript* manuscripts or any consequences arising from the use of any information contained in them.

High mobility graphene ion-sensitive field-effect transistors by noncovalent functionalization

W. Fu,^{*,†} C. Nef,[†] A. Tarasov,[†] M. Wipf,[†] R. Stoop,[†] O. Knopfmacher,^{†,‡} M. Weiss,[†] M. Calame,[†] and C. Schönenberger^{*,†}

Department of Physics, University of Basel, Klingelbergstrasse 82, CH-4056 Basel, Switzerland

E-mail: Wangyang.Fu@unibas.ch; Christian.Schoenenberger@unibas.ch

Version: September 25, 2013

Abstract

Noncovalent functionalization is a well-known nondestructive process for property engineering of carbon nanostructures, including carbon nanotubes and graphene. However, it is not clear that to what extent the extraordinary electrical properties of these carbon materials can be preserved during the process. Here, we demonstrated that noncovalent functionalization can indeed deliver graphene field-effect transistors (FET) with fully preserved mobility. And these high-mobility graphene transistors can serve as a promising platform for biochemical sensing applications.

Graphene^{1,2} has been shown to possess a variety of unique and fascinating physical and chemical properties. For example, an exceptional high carrier mobility up to $10^5 \text{ cm}^2 \text{ V}^{-1} \text{ s}^{-1}$ at room temperature, large surface-to-volume ratio, and chemical stability.³ Applications that could exploit

^{*}To whom correspondence should be addressed

[†]University of Basel

[‡]Present address: Department of Chemical Engineering, Stanford University, Stanford, California, United States

these unique properties include label-free electronic biochemical sensors with ultrahigh sensitivities.^{4–15} The sensing principle roots on a change of the electrical conductance of the transistor channel upon binding of a molecule on the sensor surface. The high sensitivity, i.e., a significant change of the electrical conductance of graphene to a minute field-effect induced by charged biochemical molecules, is explained as resulting from the extraordinary high mobility as well as low intrinsic noise in graphene.⁶ Moreover, graphene is a conductor and unique among solid state materials in that every atom is on the surface. The highest sensitivity is reached, if the conducting channel is closest to the sensor surface. Hence, if graphene is used as the conducting channel in an ion-sensitive field-effect transistor (ISFET) and at the same time as the sensing surface, the ultimate sensor could be realized.

However, due to its perfect lattice without dangling bonds, graphene is intrinsically chemically inert.^{17,18} Hence, only through the functionalization of graphene with specific recognition moieties, the sensitivity potential of graphene can be unlocked. There are actually already numerous publications on chemical functionalization of graphene, ranging from covalent to noncovalent methods, using different biochemical molecules and treatments.^{14,18–28} For example, a graphene sheet can be doped with covalent oxygen functional groups, giving graphene oxide (GO) or reduced GO (RGO) with improved sensing responses. But these methods will break the chemical bonds in the graphene lattice, inevitably leading to a severe degradation in mobility.^{14,19–21} In addition, noncovalent functionalization of graphene (or carbon nanotube) by aromatic molecules has been widely investigated for studies like the controllable doping of n- or p-type carbon-based FETs, band gap engineering, and linker molecular designing.^{25–28} Surprisingly, however, in these studies, despite noncovalent functionalization is well-known for its nondestructive features, it is not clear that to what extent the high mobility of graphene can be preserved and what detecting limit such graphene sensors can achieve. Here, by configuring the graphene FETs with aromatic molecules, we report high mobility graphene ion-sensitive FET (GISFET) H⁺ and K⁺ sensors (as well as electrostatic potential sensor) with fully preserved mobilities. The exceptional electronic quality of the unperturbed sp² graphene lattice, also ensures a potential detection limit over two or-

ders of magnitude better than that of the state-of-the-art pH meters. Undoubtedly, our achieved full mobility conservation and outstanding sensitivity of versatile GISFETs by noncovalent functionalization, will significantly increase the credibility and fidelity of graphene biochemical sensors and thus expand their application field, such as ultrasensitive environmental monitoring and medical diagnosis, especially at a high sampling rate where the mobility is of key importance.

We fabricate solution compatible graphene devices following the fabrication flow as shown in Fig. 1a. We start from monolayer graphene grown on copper foil by chemical vapor deposition (CVD).^{17,29} A square-shaped sacrificial layer (made by Parafilm (PF)/PMMA) is glued on top of the graphene/copper foil, which protects the graphene underneath during O₂ plasma etching. The sacrificial layer is then washed away in acetone. The resulting patterned graphene/copper foil is then glued onto a glass substrate up-side-down using epoxy (Epotek 302-3M, Epoxy Technology). After etching away the copper foil in an ammonium persulfate solution, the device is ready. This process is reliable and results in a graphene layer that strongly binds to the substrate and has a clean upper surface free of any resist contaminations. This last point is important because resist residues can prevent surface functionalization and suppress sensing. Such a graphene sheet is then electrically connected with silver paint at its corners, which are afterwards sealed with epoxy for operation in an electrolyte environment (Fig. 1b). Fig. 1c provides a cross-sectional view of the device together with a schematics of the electrical circuit. The gate voltage V_{Pt} was applied to the solution via a Pt wire. The electrostatic potential in solution V_{ref} was monitored by a calomel reference electrode. We have monitored the current flowing between the graphene and the liquid gate during liquid gate sweeping. This leak current never exceeded 10 nA in all our experiments. It is at least three orders of magnitude smaller than the typical source-drain current. More details on measurement can be found in Methods and our previous publication.¹⁷ Dozens of such devices were fabricated and tested. Typical results are presented.

As-fabricated graphene FETs usually exhibit a weak pH response of a few mV/pH (Supplementary Figure S1), which can be ascribed to uncontrollable and random surface defects that react with protons. These defects can be neutralized by covering the surface with fluorobenzene.¹⁷ In

contrast to the fluorobenzene passivation, we now apply a well-defined functionalization protocol that involves the π -bonding of aromatic molecules containing pH-active hydroxyl (OH) groups, phenol, to induce a significant pH response of the graphene FETs. This is done by immersing a fresh graphene FET in 1 M phenol in ethanol for 5 min and then rinsing in pure ethanol for another 5 min. To achieve a high density of the OH groups, and therefore a significant ion response, is one of the reasons why we chose phenol instead of other bigger aromatic molecules because phenol can be more densely packed. 1-Hydroxypyrene, for example, is expected to give better adhesion but has only one fourth of the active groups of phenol at the same surface coverage. The upper panel of Fig. 2a depicts the electrical transfer curves of such a phenol-activated electrolyte-gated GISFET. The plot shows the sheet conductance G_S measured as a function of the reference gate voltage V_{ref} for different pH buffer solutions (see Methods). A bipolar transistor characteristic is observed within an operation voltage range of 0.4 V. Such a characteristic reflects the fact that the type of carriers in graphene can be continuously tuned from holes (p-type region to the left in Fig. 2a) to electrons (n-type region to the right). This is realized by driving the liquid gate that controls the electrochemical potential (Fermi energy) of the charge carriers. In the following, we will focus on the transition point between the electron and hole regime, where the conductance is minimal. This point is also referred to as the charge-neutrality point (CNP). The shift of V_{CNP} against pH is defined as the pH response of the sensor. We note here that measurements of such functionalized GISFETs show an excellent degree of reproducibility and stability (Supplementary Figure S1). Remarkably, the transfer curves for this phenol-activated GISFET (Fig. 2a, top panel) shift significantly when the pH is changed. The shift of the phenol-activated GISFET contrasts with the nicely overlapping curves for the passivated graphene FET (bottom panel). This passivation is achieved by coating the graphene surface with aromatic molecules that contain passive groups such as fluorobenzene using a similar protocol (see Methods). In the following, we will quantify the shifts in detail. Note, here that the minimum sheet conductance G_{S-min} for fluorobenzene-passivated and phenol-activated graphene FETs are $4.7 e^2/h$ and $3.6 e^2/h$, respectively, which is on the order of $4 e^2/h$ as expected for monolayer graphene.¹

In Fig. 2b, $\Psi_0 = V_{CNP}(pH) - V_{CNP}(pH = 3)$ is depicted as a function of pH for the two different functionalizations, where Ψ_0 is defined as the surface potential of GISFETs. For the fluorobenzene passivation (squares in Fig. 2b), an inert behavior is observed, with a sensitivity less than 1 mV/pH (the slope of the linear fit). This result is in agreement with our recent report,¹⁷ showing that the clean hydrophobic graphene surface does not coordinate protons. The graphene FET decorated with phenol molecules, on the other hand, exhibits a nonlinear pH response. It is flat at the beginning and rises with a striking response of 49 mV/pH at pH larger than 8, which compares favorably with the measured pH response (30 – 60 mV/pH) of Si-based ISFETs with oxide surfaces (SiO₂, Al₂O₃, HfO₂, etc.). As a control, we have also studied the pH response of GISFETs with hybrid fluorobenzene and phenol functionalizations (Supplementary Figure S2). We demonstrated that a reduced number of adsorbed pH-active phenol molecules weakens the pH response of the GISFETs, suggesting unambiguously that the proton sensitivity of the GISFETs originates from the adsorbed phenol molecules. Further confirmation of phenol adsorption comes from quartz crystal microbalance (QCM) measurements as will be discussed later (see also Methods).

The aromatic functionalization does not only endow the GISFET with a significant pH response, but also preserves the electronic quality of graphene that is commonly characterized by the charge carrier mobility. As reported in previous literatures, we also observe almost identical Raman spectrum of graphene before and after aromatic molecular adsorption (not shown here), indicating a non-destructive functionalization. Here, as a significant demonstration in comparison to previous reports, we directly evaluate the mobility of graphene from the slope of the linear regimes of $G(n)$ as $\mu = \delta G / e \delta n$, where the carrier mobility n is obtained by converting the gate voltage V_{ref} (Supplementary Figure S3). We confirm that the carrier mobility extracted from this method matches that obtained from Hall effect measurements (Supplementary Figure S3). The reliability of this method also roots in the reproducible and stable transfer characteristics of our fabricated GFETs with clean surface, which are dedicated for liquid environment sensing applications. The hole and electron mobility of this phenol-activated GISFET were found to be 1770 cm²V⁻¹s⁻¹ and 2020 cm²V⁻¹s⁻¹, respectively. These mobilities, as well as those of the fluorobenzene-passivated

graphene FET ($2650 \text{ cm}^2\text{V}^{-1}\text{s}^{-1}$ for hole and $3260 \text{ cm}^2\text{V}^{-1}\text{s}^{-1}$ for electron), are at least more than one order of magnitude higher than that of high-performance silicon ISFETs^{30,31} formed on SOI wafers, which only have a peak hole mobility of $137 \text{ cm}^2\text{V}^{-1}\text{s}^{-1}$. The same is true for ISFETs based on GO/RGO or organic polymers with mobility on the order of $10 \text{ cm}^2\text{V}^{-1}\text{s}^{-1}$ or even less.^{19,32} Furthermore, we have also recorded the transfer curves of the same graphene FETs before aromatic functionalization. For instance, the hole and electron mobility of the graphene FET before fluorobenzene adsorption, were $2630 \text{ cm}^2\text{V}^{-1}\text{s}^{-1}$ and $3140 \text{ cm}^2\text{V}^{-1}\text{s}^{-1}$, respectively, with a minimum sheet conductance $G_{S-min} = 195 \mu\text{S} = 5.1 e^2/h$. Obviously, the addition of aromatic molecules has preserved both the high mobility and the high conductivity of the graphene FET devices, as summarized in Tab. 1 for 6 different samples with 3 different kinds of aromatic functionalizations. This picture immediately leads to the conclusion that functionalization with aromatic molecules has a great advantage. Adding aromatic molecules that contain OH groups (for example) to the graphene surface induces the high pH response. At the same time, the extraordinary high carrier mobility, thus the excellent electrical properties of graphene, have been fully preserved. In practice, this functionalization approach renders GISFET as a perfect platform for sensing applications, especially at a high sampling rate where the mobility is of key importance. We note here that, in some of the graphene FET devices, there is a noticeable increase in the mobility after aromatic functionalization. Further investigations are required to identify the underlying mechanism.

It is clear that graphene based ISFETs have extraordinary high carrier mobility. The resulting high transconductance will endow the sensors with significant current response to minute changes in the surface potential (caused by the adsorption of molecules). However, inherent noise, especially low-frequency $1/f$ noise, which is ubiquitous in solid-state electronic devices, sets a limit on the size of the signal that can be detected. This noise can be measured and characterized by using well-established techniques in the MOSFET community. Therefore noise measurement and characterization represent valuable tools for predicting the detection limit of biochemical FET sensors. Here we measured the low frequency noise spectrum of the graphene FETs (Supplementary

Figure S4). When related to a shift in the CNP, we found $\delta V_{CNP}(10 \text{ Hz}) = 1.8 \times 10^{-7} \text{ V/Hz}^{\frac{1}{2}}$ for the phenol-activated GISFET. The input noise δV_{CNP} can be regarded as the resolution limit of this sensor, which corresponds to a measurement accuracy of 4 ppm of a pH shift in 1 Hz bandwidth. This result is over two orders of magnitudes better than that of the state-of-the-art commercial pH sensors [1,000 ppm (Ref. 33)]. This is not a surprise. As we found recently, the highest sensitivity of an ISFET is reached, if its conducting channel is closest to the sensor surface.¹⁶ And this requirement is fulfilled in our graphene ISFETs.

We note that the transfer curves of the phenol-activated GISFET shift to positive gate voltages with increasing pH values. This behavior is expected for phenol containing active OH groups that can be deprotonized as a weak acid: $C_6H_5OH \rightleftharpoons C_6H_5O^- + H_s^+$, with H_s^+ denoting surface protons. At high pH values, the equilibrium is shifted towards a deprotonized surface which is negatively charged. As a consequence, the transfer curve is expected to shift to the right. Based on this sensing mechanism, we can derive a relation between the surface potential Ψ_0 of the graphene FET and the pH value of the bulk solution (Supplementary Eq. S2-8):

$$pH = -\log[-K_a \cdot \exp\left(\frac{e\Psi_0}{kT}\right) \cdot \left(1 + \frac{eN_s}{C_{dl}\Psi_0}\right)].$$

Here, k denotes the Boltzmann constant, $T = 300 \text{ K}$ the absolute temperature, and $C_{dl} = 2 \times 10^{-1} \text{ Fm}^{-2}$ the double-layer capacitance. K_a and N_s represent the equilibrium constant and the density of the surface active phenol molecules, respectively.

The non-linear data points in Fig. 2b can be nicely described by using the equation above with K_a and N_s two free fitting parameters. As a result, we deduce the equilibrium constant K_a of phenol (adsorbed on graphene surface) to be $10^{-8.6} \text{ M}$ (as confirmed in SI, Figure S2c). This surface K_a is consistent with the literature value of $10^{-9.98} \text{ M}$ measured in bulk solution.³⁴ Differences are most probably caused by solution versus surface-bound measurements, i.e., the acidity of phenol increases due to its electron donating to graphene. The fitting to the data yield $N_s = 5.5 \times 10^{14} \text{ cm}^{-2}$. This number is in good agreement with QCM measurements (see Methods). The density of ac-

tivated surface groups N_s is the key parameter in determining the pH response of the GISFETs. The high sensitivity of the GISFET to pH is only possible if the surface contains active sites of a very high density. We have achieved $N_s = 5.5 \times 10^{14} \text{ cm}^{-2}$, which corresponds to 5.5 active hydroxyl groups in an area of $1 \text{ nm} \times 1 \text{ nm}$. This value is comparable with the literature value for oxide surfaces ($5 \times 10^{14} \text{ cm}^{-2}$ for SiO_2 and $8 \times 10^{14} \text{ cm}^{-2}$ for Al_2O_3).^{35–39}

Up to now, we have investigated the pH sensing response of GISFETs functionalized by aromatic molecules. To demonstrate that GISFETs can detect ions other than protons, we chose the high-affinity 18-crown-6-potassium cation system. The binding of the crown ether to potassium cation has been studied in detail, and an equilibrium constant of $10^{-2.03} \text{ M}$ was measured in aqueous solution.⁴⁰ As shown in the upper left of Fig. 3, a crown ether was chosen which can be anchored onto graphene by the benzene linkers via π - π stacking (see Methods). Note, as fabricated graphene FETs exhibit only a weak potassium ion (as well as pH) sensitivity (-3 mV/pK , not shown here).

After functionalization, potassium cations could bind to crown ether and the sensor response of the potassium GISFET was recorded. Fig. 3 illustrates the conductivity of a crown ether activated GISFET device tested in a KCl solution in water with different concentrations ranging from $100 \mu\text{M}$ to 1 M . Note here that the position of the CNP now shifts toward negative potentials with increasing ion concentration. The shift of the V_{CNP} is plotted in the inset as a function of pK, which is the the negative logarithm of its activity a_{KCl} . The negative shift can be explained by the adsorption of positive potassium ions.^{8,9} In this case, the mechanism can be described analytically using a single-reaction model similar to the phenol case above (Supplementary Eq. S9). The result quantitatively accounts for the data points in the inset of Fig. 3 (red line). Likewise, we can extract a density of adsorbed effective crown ether of $9 \times 10^{12} \text{ cm}^{-2}$ and an equilibrium constant of $10^{-2.3} \text{ M}$, which is close to that ($10^{-2.03} \text{ M}$) of 18-crown-6 measured in bulk solution (the difference is probably due to solution versus surface-bound measurements). We would like to stress that the extracted mobility and channel conductivity show no degradation after functionalization (see Tab.1) also for this sensing prototype.

In summary, by using aromatic functionalization, we demonstrated H⁺ and K⁺ GISFETs with fully preserved mobilities and promising ion sensitivities. Importantly, the noncovalent modification method preserves the excellent electrical properties of graphene and allows for the development of high-performance graphene sensors. For example, an exceptional low pH detection limit that is over two orders of magnitude better than that of the state-of-the-art pH meters, has been evaluated by means of noise measurement. Based on these findings, we are truly convinced that graphene holds great promise for sensing applications, such as environmental monitoring and medical diagnosis, especially at a high sampling rate where the mobility is of key importance.

Experimental Section

CVD graphene growth. Graphene films were grown on 25- μ m thick copper foils (99.8 %, Alfa Aesar, item No. 13382) in a split quartz tube furnace using a CVD method involving methane and hydrogen gases, whose flow rates were precisely controlled by mass flow controllers. Under base vacuum conditions of 40 mTorr, the furnace was heated with a 10 sccm flow of hydrogen. After reaching the growth temperature, we waited 20 min to allow the copper foil to anneal. For our optimized growth step, the chamber conditions were: CH₄:H₂ gas flow of 25:10 sccm, pressure of 1.5 Torr, and a temperature of 1,000 °C. When the growth was finished, the hydrogen gas flow was kept during fast cool down (100 °C/min).

Characterization. The transistor characteristics of the graphene FET devices in different solutions were tested automatically in a home-made setup. The corner contacts can be numbered from 1 to 4 in a clockwise order (here the beginning corner is arbitral since the sample is symmetrical). A Keithley 2600A was used as the source meter to inject a current flow I_{12} in graphene layer between two adjacent corners 1 and 2. The voltage drop between another two adjacent corners, V_{34} , was collected using a Keithley nanovolt meter 2800. The sheet conductance of graphene sheet can then be calculated as: $G_S = \frac{\ln 2}{\pi} \cdot \frac{I_{12}}{V_{34}}$. The reference voltage V_{ref} was monitored with a Keithley multimeter 3600.

Sample functionalization and solution preparation. The fluorobenzene passivated graphene FET sample was prepared by immersing the device in pure fluorobenzene liquid for 30 s and blow drying. By immersing the fresh graphene FET device in 1 M phenol in ethanol for 5 min and rinsing in pure ethanol for another 5 min and blow drying, we achieved the phenol-activated GISFET sample. The crown ether-activated GISFET was prepared by functionalizing the graphene sample in 0.1 M solution of dibenzo-18-crown-6-ether in chloroform for 5 min and rinsing in pure ethanol for another 5 min and blow drying. As for electrolyte, we used standard pH buffer solutions (Trisitol pH 2-9, Merck) and KCl solutions made by dissolving the salts in deionized water. The pH values [monitored by pH strips and a glass electrode (691 pH Meter, Metrohm)] of the KCl solutions remained constant at $\text{pH} \cong 5.5$ over the concentration range we discuss in this paper.

QCM measurements. QCM measures a mass per unit area by monitoring the change in frequency of a quartz crystal resonator. Here we started from QCM sensors with Au active electrode. CVD graphene was transferred onto the sensors and resulting in QCM sensors with graphene active electrode. In order to achieve a clean graphene surface, a post annealing in Ar/H₂ gas was performed at 300 °C for 1 h. The resonate frequency of such QCM sensors was then monitored both before and after functionalizations. The change in frequency was recorded and converted into adsorbed mass per unit area by using the Sauerbrey relation: $\Delta m = \frac{C\Delta f}{n}$, where $C = 17.7 \text{ ngcm}^{-2}\text{s}$ is a constant and $n = 3$ denotes the overtone of the quartz crystal that we monitored. For the fluorobenzene and phenol functionalizations, the QCM measurements gave adsorbed density of $5.7 \times 10^{14} \text{ cm}^{-2}$ and $7.5 \times 10^{14} \text{ cm}^{-2}$ after thoroughly rinsing, respectively.

Acknowledgements

The authors acknowledge funding from the Swiss Nanoscience Institute (SNI), nanotera.ch, Swiss NSF via the Sinergia program (126969), the ESF programme Eurographene, and the European Commission under the FP7-NMP project Hysens (263091).

References

- (1) K. S. Novoselov, A. K. Geim, S. V. Morozov, D. Jiang, Y. Zhang, S. V. Dubonos, I. V. Grigorieva, A. A. Girsov, Electric Field Effect in Atomically Thin Carbon Films. *Science* **2004**, *306*, 666-669.
- (2) K. S. Novoselov, D. Jiang, F. Schedin, T. J. Booth, V. V. Khotkevich, S. V. Morozov, A. K. Geim, Two-Dimensional Atomic Crystals. *Proc. Natl. Acad. Sci. U. S. A.* **2005**, *102*, 10451-10453.
- (3) S. Das Sarma, S. Adam, E. H. Hwang, E. Rossi, Electronic transport in two dimensional graphene. *arXiv:1003.4731v2* (2010).
- (4) P. K. Ang, W. Chen, A. T. S. Wee, K. P. Loh, Solution-Gated Epitaxial Graphene as pH Sensor. *J. Am. Chem. Soc.* **2008**, *130*, 14392-14393.
- (5) J. Ristein, W. Y. Zhang, F. Speck, M. Ostler, L. Ley, T. Seyller, Characteristics of solution gated field effect transistors on the basis of epitaxial garphene on silicon carbide. *J. Phys. D: Appl. Phys.* **2010**, *43*, 345303.
- (6) Z. G. Cheng, Q. Li, Z. J. Li, Q. Y. Zhou, Y. Fang, Suspended Graphene Sensors with Improved Signal and Reduced Noise. *Nano Lett.* **2010**, *10*, 1864-1868.
- (7) Y. Ohno, K. Maehashi, Y. Yamashiro, K. Matsumoto, Electrolyte-Gated Graphene Field-Effect Transistors for Detecting pH and Protein Adsorption. *Nano Lett.* **2009**, *9*, 3318-3322.
- (8) I. Heller, S. Chatoor, J. Männik, M. A. G. Zevenbergen, C. Dekker, S. G. Lemay, Influence of Electrolyte Composition on Liquid-Gated Carbon Nanotube and Graphene Transistors. *J. Am. Chem. Soc.* **2010**, *132*, 17149-17156.
- (9) F. Chen, Q. Qing, J. Xia, J. Li, N. Tao, Electrochemical Gate-Controlled Charge Transport in Graphene in Ionic Liquid and Aqueous Solution. *J. Am. Chem. Soc.* **2009**, *131*, 9908-9909.

- (10) J. L. Xia, F. Chen, P. Wiktor, D. K. Ferry, N. J. Tao, Effect of Top Dielectric Medium on Gate Capacitance of Graphene Field Effect Transistors: Implications in Mobility Measurements and Sensor Applications. *Nano Lett.* **2010**, *10*, 5060-5064.
- (11) M. Dankerl, M. V. Hauf, A. Lippert, L. H. Hess, S. Birner, I. D. Sharp, A. Mahmood, P. Mallet, J. Y. Veullen, M. Stutzmann, J. A. Garrido, Graphene Solution-Gated Field-Effect Transistor Array for Sensing Applications. *Adv. Funct. Mater.* **2010**, *20*, 3117-3124.
- (12) T. Cohen-Karni, Q. Qing, Q. Li, Y. Fang, C. M. Lieber, Graphene and Nanowire Transistors for Cellular Interfaces and Electrical Recording. *Nano Lett.* **2010**, *10*, 1098-1102.
- (13) Z. L. Mišković, N. Upadhyaya, Modeling Electrolytically Top-Gated Graphene. *Nanoscale Res. Lett.* **2010**, *5*, 505-511.
- (14) S. J. Park, O. S. Kwon, S. H. Lee, H. S. Song, T. H. Park, J. Jang, Ultrasensitive Flexible Graphene Based Field-Effect Transistor (FET)-Type Bioelectronic Nose. *Nano Lett.* **2012**, *12*, 5082-5090.
- (15) F. Yavari, N. Koratkar, Graphene-Based Chemical Sensors. *J. Phys. Chem. Lett.* **2012**, *3*, 1746-1753.
- (16) K. Bedner, V. A. Guzenko, A. Tarasov, M. Wipf, R. L. Stoop, J. Brunner, W. Fu, R. A. Minamisawa, C. David, M. Calame, J. Gobrecht, C. Schönenberger, Scaling of Noise Limitations in Silicon Nanowire Charge Sensors. *to be submitted*.
- (17) W. Fu, C. Nef, O. Knopfmacher, A. Tarasov, M. Weiss, M. Calame, C. Schönenberger, Graphene Transistors Are Insensitive to pH Changes in Solution. *Nano Lett.* **2011**, *11*, 3597-3600.
- (18) Y. Lu, B. R. Goldsmith, N. J. Kybert, A. T. C. Johnson, DNA-Decorated Graphene Chemical Sensors. *Appl. Phys. Lett.* **2010**, *97*, 083107.

- (19) Y. Liu, X. Dong, P. Chen, Biological and Chemical Sensors Based on Graphene Materials. *Chem. Soc. Rev.* **2012**, *41*, 2283-2307.
- (20) J. T. Robinson, F. K. Perkins, E. S. Snow, Z. Wei, P. E. Sheehan, Reduced Graphene Oxide Molecular Sensors. *Nano Lett.* **2008**, *8*, 3137-3140.
- (21) J. D. Fowler, M. J. Allen, V. C. Tung, Y. Yang, R. B. Kaner, B. H. Weiller, Practical Chemical Sensors from Chemically Derived Graphene. *ACS Nano* **2009**, *3*, 301-306.
- (22) T. Zhang, Z. Cheng, Y. Wang, Z. Li, C. Wang, Y. Li, Y. Fang, Self-Assembled 1-Octadecanethiol Monolayers on Graphene for Mercury Detection. *Nano Lett.* **2010**, *10*, 4738-4741.
- (23) Y. Cui, S. N. Kim, S. E. Jones, L. L. Wissler, R. R. Naik, M. C. McAlpine, Chemical Functionalization of Graphene Enabled by Phage displayed Peptides. *Nano Lett.* **2010**, *10*, 4559-4565.
- (24) J. Katoch, S. N. Kim, Z. Kuang, B. L. Farmer, R. R. Naik, S. A. Tatulian, M. Ishigami, Structure of a Peptide Adsorbed on Graphene and Graphite. *Nano Lett.* **2012**, *12*, 2342-2346.
- (25) H. C. Cheng, R. J. Shiue, C. C. Tsai, W. H. Wang, Y. T. Chen, High-Quality Graphene p-n Junctions via Resist-free Fabrication and Solution-Based Noncovalent Functionalization. *ACS Nano* **2011**, *5*, 2051-2059.
- (26) Z. Zhang, H. Huang, X. Yang, L. Zang, Tailoring Electronic Properties of Graphene by π - π Stacking with Aromatic Molecules. *J. Phys. Chem. Lett.* **2011**, *2*, 2897-2905.
- (27) V. K. Kodali, J. Scimgeour, S. Kim, J. H. Hankinson, K. M. Carroll, W. A. de Heer, C. Berger, J. E. Curtis, Nonperturbative Chemical Modification of Graphene for Protein Micropatterning. *Langmuir* **2011**, *27*, 863-865.
- (28) H. Wang, X. Wang, X. Li, H. Dai, Chemical self-assembly of graphene sheets. *Nano Res.* **2009**, *2*, 336-342.

- (29) X. S. Li, W. W. Cai, J. An, S. Kim, J. Nah, D. X. Yang, R. Piner, A. Velamakanni, I. Jung, E. Tutuc, S. K. Banerjee, L. Colombo, R. S. Ruoff, Large-Area Synthesis of High-Quality and Uniform Graphene Films on Copper Foils. *Science* **2009**, *324*, 1312-1314.
- (30) E. Stern, J. F. Klemic, D. A. Routenberg, P. N. Wyrembak, D. B. Turner-Evans, A. D. Hamilton, D. A. LaVan, T. M. Fahmy, M. A. Reed, Label-free immunodetection with CMOS-compatible semiconducting nanowires. *Nature* **2007**, *445*, 519-522.
- (31) S. Chen, J. G. Bomer, E. T. Carlen, A. van den Berg, Al₂O₃/Silicon NanoISFET with Near Ideal Nernstian Response. *Nano Lett.* **2011**, *11*, 2334-2341.
- (32) A. Dodabalapur, Organic and Polymer Transistors for Electronics. *Mater. Today* **2006**, *9*, 24-30.
- (33) Microsens SA, http://www.microsens.ch/products/pdf/MSFET_datasheet%20.pdf (retrieved 17 September 2010) A. Tarasov, W. Fu, O. Knopfmacher, J. Brunner, M. Calame, C. Schönenberger, Signal-to-Noise Ratio in Dual-Gated Silicon Nanoribbon Field-Effect Sensors. *Appl. Phys. Lett.* **2011**, *98*, 012114.
- (34) K. C. Gross, P. G. Seybold, Substituent Effects on the Physical Properties and pK_a of Phenol. *Int. J. Quant. Chem.* **2001**, *85*, 569-579.
- (35) L. Bousse, N. F. De Rooij, P. Bergveld, Operation of Chemically Sensitive Field-Effect Sensors As a Function of the Insulator-Electrolyte Interface. *IEEE Trans. Electron Dev.* **1983**, *ED-30*, 1263-1270.
- (36) P. Bergveld, Thirty years of ISFETOLOGY. *Sens. Actuators B* **2003**, *88*, 1-20.
- (37) S. Y. Chen, J. G. Bomer, W. G. van der Wiel, E. T. Carlen, A. van den Berg, Top-Down Fabrication of Sub-30 nm Monocrystalline Silicon Nanowires Using Conventional Microfabrication. *ACS Nano* **2009**, *3*, 3485-3492.

- (38) A. Tarasov, M. Wipf, K. Bedner, J. Kurz, W. Fu, V. A. Guzenko, O. Knopfmacher, R. L. Stoop, M. Calame, C. Schönenberger, A True Reference Nanosensor Realized with Silicon Nanowires. *Langmuir* **2012**, *28*, 9899-9905.
- (39) O. Knopfmacher, A. Tarasov, W. Y. Fu, M. Wipf, B. Niesen, M. Calame, C. Schönenberger, Nernst Limit in Dual-Gated Si-Nanowire FET Sensors. *Nano Lett.* **2010**, *10*, 2268-2274.
- (40) G. W. Gokel, W. M. Leevy, M. E. Weber, Crown Ethers: Sensors for Ions and Molecular Scaffolds for Materials and Biological Models. *Chem. Rev.* **2004**, *104*, 2723-2750.

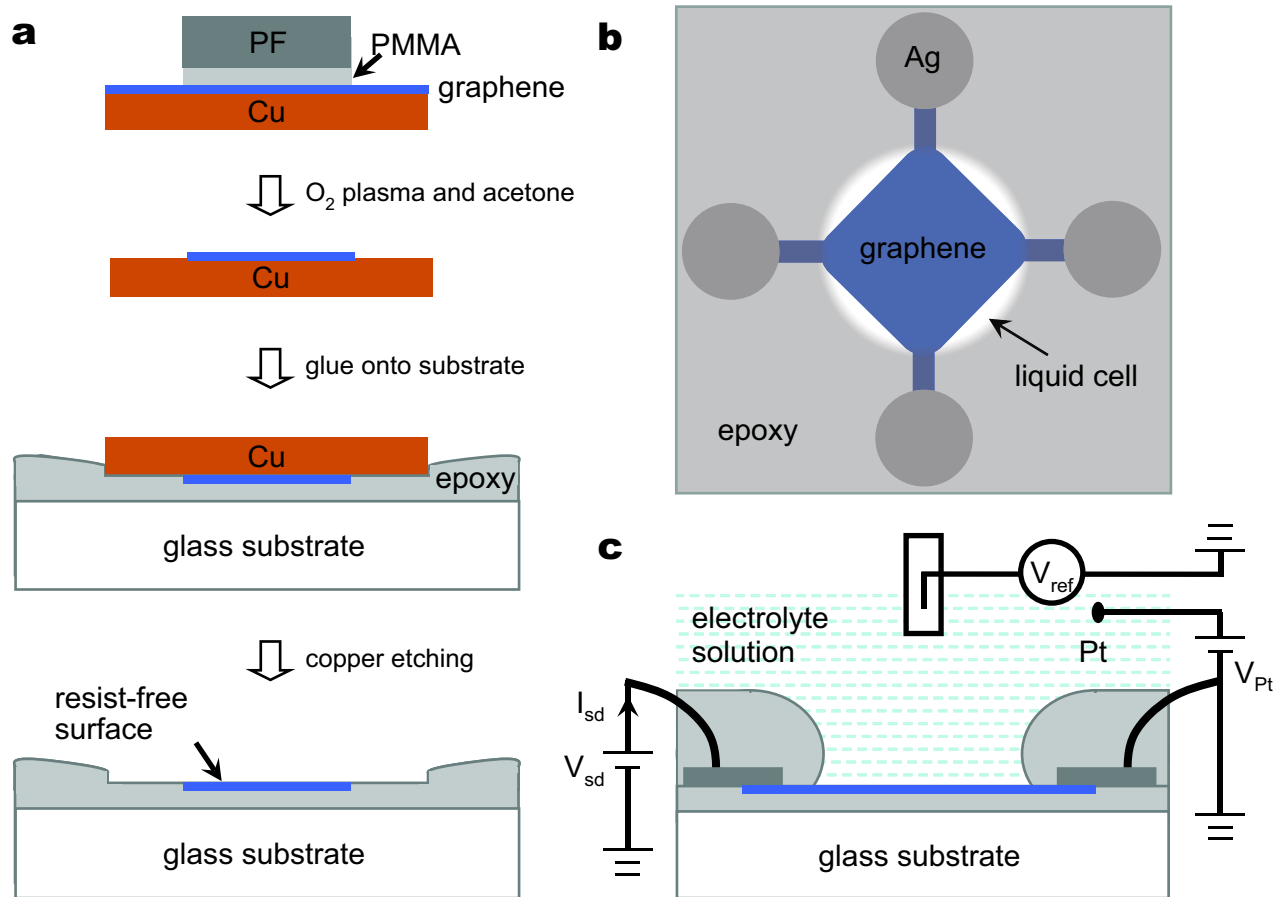


Fig. 1. Graphene FET fabrication and measurement scheme. (a) Process flow for patterning and transferring a CVD graphene sheet (blue) with clean surface. (b) Schematic of a fabricated graphene FET with liquid sealing (top view). (c) Schematic of the experimental setup and the electrical circuitry of the electrolyte-gated graphene FET. The gate voltage V_{Pt} was applied to the solution via a Pt wire. The electrostatic potential in solution was monitored by a commercial calomel reference electrode as V_{ref} .

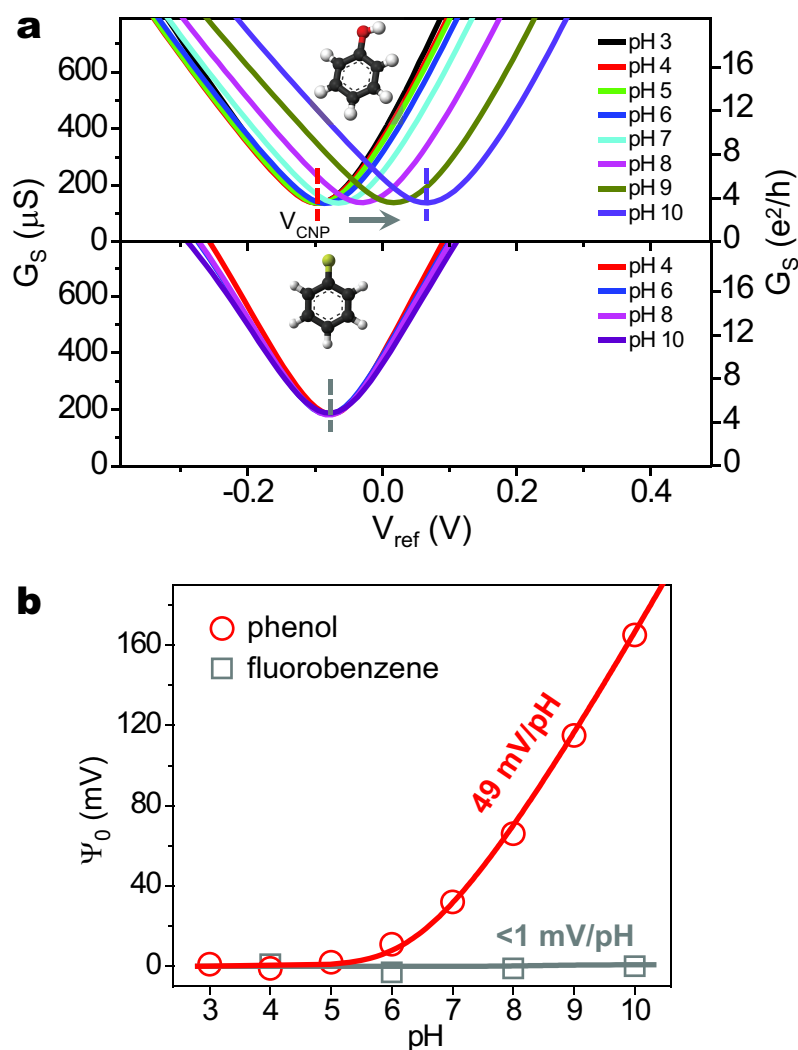


Fig. 2. pH responses of graphene FETs with phenol and fluorobenzene functionalizations. (a) Electrical sheet conductance G_S as a function of the reference potential V_{ref} measured in different pH buffer solutions for the phenol-activated (top) and fluorobenzene-passivated (bottom) graphene FETs. Inset: molecular structure of phenol (top) and fluorobenzene (bottom). Black, white, red, and green correspond to carbon, hydrogen, oxygen, and fluorine atoms, respectively. (b) Change of the surface potential Ψ_0 of graphene FETs vs pH of the buffer solution with phenol and fluorobenzene functionalizations. The red curve is a fit to the single-reaction model with an equilibrium constant of $10^{-8.6}$ M and an active group density of 5.5×10^{14} cm $^{-2}$.

GFET functionalizations	hole mobility ($\text{cm}^2\text{V}^{-1}\text{s}^{-1}$)		electron mobility ($\text{cm}^2\text{V}^{-1}\text{s}^{-1}$)		minimum conductance (μS)	
	<i>before</i>	<i>after</i>	<i>before</i>	<i>after</i>	<i>before</i>	<i>after</i>
fluorobenzene: ref	*2630	2650	3140	3260	195	180
phenol: pH sensor	*2050	1770	2590	2020	205	140
	1180	1360	1920	1800	310	240
	260	380	270	310	90	105
crown ether: K^+ sensor	*270	340	210	310	~615	~630
	1090	1270	1870	1520	280	300

* : also discussed in the main manuscript

Tab. 1. The calculated carrier mobilities as well as the minimum conductances of six as-fabricated and functionalized graphene FETs.

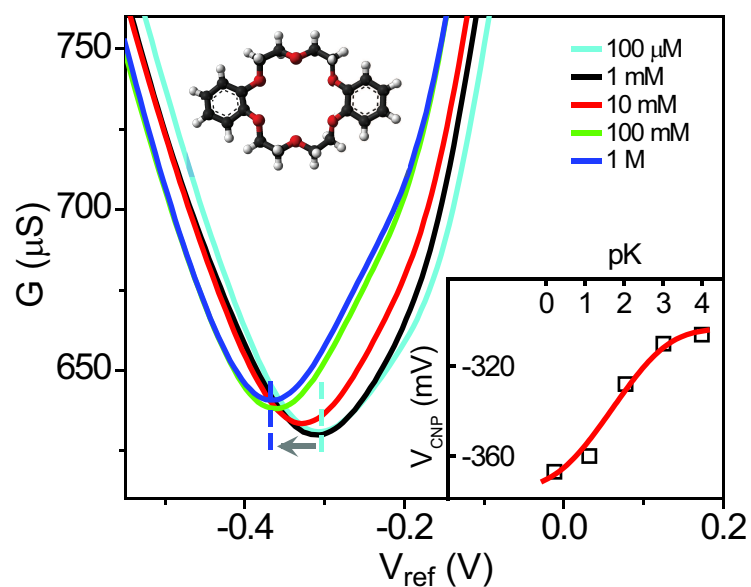
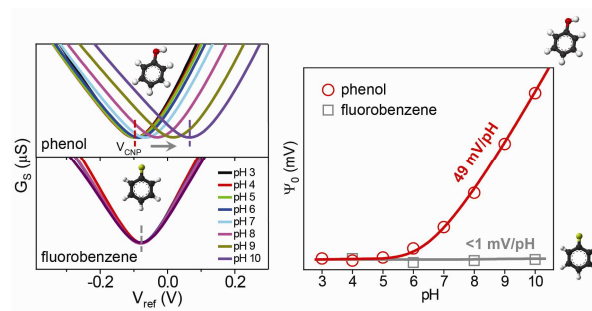


Fig. 3. Response of a crown ether-functionalized GISFET to K^+ ions. The electrical source-drain conductance G is depicted as a function of the reference potential V_{ref} in different KCl solutions. Lower right inset: change of the GISFET's V_{CNP} vs pK of the KCl solution. The red curve is a fit to the single-reaction model with an equilibrium constant of $10^{-2.3}$ M and an active group density of $9 \times 10^{12} \text{ cm}^{-2}$. The molecular structure of dibenzo-18-crown-6-ether is shown as the top left inset. Black, white, and red represent carbon, hydrogen, and oxygen atoms, respectively.



A significant pH response of the graphene FETs can be achieved by using aromatic functionalization.